Journal of Theoretical Biology 334 (2013) 1–12

Contents lists available at SciVerse ScienceDirect

Journal of Theoretical Biology

journal homepage: www.elsevier.com/locate/yjtbi

Modelling biological invasions: Individual to population scales at interfaces

J. Belmonte-Beitia [a,*,1], T.E. Woolley [b,c,1], J.G. Scott [c,d], P.K. Maini [c], E.A. Gaffney [c]

[a] Departamento de Matemáticas, E. T. S. de Ingenieros Industriales, Universidad de Castilla-La Mancha 13071 Ciudad Real, Spain
[b] Oxford Centre for Collaborative Applied Mathematics, Mathematical Institute, University of Oxford, 24–29 St Giles', Oxford, OX1 3LB, UK
[c] Centre for Mathematical Biology, Mathematical Institute, University of Oxford, 24–29 St Giles', Oxford, OX1 3LB, UK
[d] Integrated Mathematical Oncology, H Lee Moffitt Cancer Center and Research Institute, Tampa, FL 33612, USA

HIGHLIGHTS

- We explore the influence of spatial heterogeneity in biological systems.
- We consider how local transport mechanisms impact behaviour near interfaces.
- We study cell movement between white and grey matter in the brain, as an example.
- Profound differences in population behaviour emerge in the presence of interface.
- The commonly used Fickian diffusion transport model cannot predict this dynamics.

ARTICLE INFO

Article history:
Received 25 October 2012
Received in revised form
24 May 2013
Accepted 28 May 2013
Available online 13 June 2013

Keywords:
Fisher equation
Stochastic process
Heterogeneous diffusion
Glioma
Tumor invasion

ABSTRACT

Extracting the population level behaviour of biological systems from that of the individual is critical in understanding dynamics across multiple scales and thus has been the subject of numerous investigations. Here, the influence of spatial heterogeneity in such contexts is explored for interfaces with a separation of the length scales characterising the individual and the interface, a situation that can arise in applications involving cellular modelling. As an illustrative example, we consider cell movement between white and grey matter in the brain which may be relevant in considering the invasive dynamics of glioma. We show that while one can safely neglect intrinsic noise, at least when considering glioma cell invasion, profound differences in population behaviours emerge in the presence of interfaces with only subtle alterations in the dynamics at the individual level. Transport driven by local cell sensing generates predictions of cell accumulations along interfaces where cell motility changes. This behaviour is not predicted with the commonly used Fickian diffusion transport model, but can be extracted from preliminary observations of specific cell lines in recent, novel, cryo-imaging. Consequently, these findings suggest a need to consider the impact of individual behaviour, spatial heterogeneity and especially interfaces in experimental and modelling frameworks of cellular dynamics, for instance in the characterisation of glioma cell motility.

1. Introduction

One of the major themes in current biological modelling is the development of theoretical frameworks which allow the investigation of systems characterised by multiple length scales. For instance, in ecology, this is motivated by assessing the impact of individual and species' behaviour on large scale ecosystems, while physiological modelling ultimately demands consideration of interactions ranging from the genome to the organism.

However, the combinatorics of extrapolating population scale observations from individual dynamics typically necessitate the consideration of asymptotic representations at larger length scales. The simplest, and textbook, exemplar is that of an ensemble of unbiased random walkers in a homogeneous environment, be they cells in physiology or animals in ecology, which exhibit diffusive behaviour at the population level. This has been generalised in numerous investigations, for example in off-lattice models (Lipkova et al., 2011), whereby the framework at the individual level does not rely upon a discretisation of space and/or time, as well as the incorporation of numerous physical and biological

* Corresponding author. Tel.: +34 91926832589.
E-mail address: juan.belmonte@uclm.es (J. Belmonte-Beitia).
[1] Equal first authors.

0022-5193/$ - see front matter © 2013 Elsevier Ltd. All rights reserved.
http://dx.doi.org/10.1016/j.jtbi.2013.05.033

features. Examples in this popular field (Chowdhury et al., 2005; Othmer and Stevens, 1997; Hillen and Othmer, 2000; Deroulers et al., 2009) include the consideration of exclusion processes (Landman and Fernando, 2011), motility biases such as chemotaxis (Hillen and Painter, 2009), competing cell populations (Penington et al., 2011), contact interactions (Lushnikov et al., 2008; Painter and Sherratt, 2003) and cell–cell adhesions (Stein et al., 2007).

In particular, the importance of considering spatial heterogeneity in ecological dispersal has been emphasised in studies where the pattern and scale of movement have been characterised, for instance the dispersal of forest beetles (Turchin and Thoeny, 1993; Cronin et al., 2000), and is regularly considered in cellular modelling, which is our focus below. Consequently, the influence of spatial heterogeneity on randomly walking ensembles of individuals has been derived for a variety of contexts with, for example, Painter and Sherratt (2003), as well as Othmer and Stevens (1997), presenting numerous continuum limits. Fickian diffusion, which is ubiquitously invoked in modelling studies at the cellular scale (Murray, 2003), in fact requires non-local sensing in the presence of small scale heterogeneity (Painter and Sherratt, 2003). Ultimately, cells are not point particles, so non-local sensing has been incorporated into numerous models of dispersion, especially those involving cellular mechanics and mechano-sensing (e.g. Murray, 2003; Murray et al., 1988; Moreo et al., 2010). However, in homogeneous media, the subtlety of whether nearest neighbour non-local sensing is present or absent typically does not emerge at the population level in models that do not consider mechanics; this is in distinct contrast to environments possessing spatial heterogeneity, as illustrated below.

A fundamental example of where such a modelling application may be relevant at the cellular scale is the consideration of glioma, which is the most common adult primary brain malignancy and possesses an infiltrative behaviour; in its most aggressive state, glioblastoma, this tumour is characterised by life expectancies of less than 2 years from diagnosis and has no cure (Stupp et al., 2009). Hence, an extensive literature has developed with the purpose of assessing the spread of malignant glial cells given clinical imaging data (Swanson et al., 2002a, 2002b; Hatzikirou et al., 2005; Ellingson et al., 2011; Konukoglu et al., 2010a; Kim et al., 2009; Bearer et al., 2009; Eikenberry et al., 2009), utilising modelling frameworks that exploit the fact that these cells are highly motile and dispersive, which has been observed and even quantified *in vitro* and *in vivo* (Chicoine and Silbergeld, 1995). Quantitative comparisons with Fickian diffusion have also exhibited favourable agreement for malignant glial cells within a collagen gel, on supplementing the theoretical model with cell proliferation and a distinction between the glioma core and its invasive rim, which allows for cell shedding dynamics (Stein et al., 2007). In addition, and as recognised in current modelling frameworks (Konukoglu et al., 2010a, 2010b; Rockne et al., 2008), invading gliomas infiltrate highly heterogeneous brain tissue, due to the presence of disparate levels of myelin within white and grey matter. This, in turn, result in substantially different motilities estimated for each of these two phases, differing by a factor of between 5 and 25 according to the parameter estimation method (Rockne et al., 2008; Konukoglu et al., 2010b), with faster motility in white matter.

Our objective is to consider how local transport mechanisms impact population behaviours near interfaces, comparing and contrasting studies of interfacial behaviours for Fickian diffusion and population level representations of locally sensing individual transport. A specific illustrative context will consider the scales involved with glioma invasive dynamics in white and grey matter though, more generally, we are exploring how interfacial architecture interplays with cellular behaviour to influence population level predictions, given a separation of length scales for the individual, the interface and the population.

2. Cellular level dynamics in the presence of spatial heterogeneity

We briefly review the derivation of equations describing the population level dynamics of individuals that are random walkers and sense only locally, which we refer to as myopic walkers below, with a generalisation to the sensing required for Fickian diffusive dynamics. We also briefly describe how to perform simulations incorporating the stochasticity for these systems to allow a study of the influence of intrinsic noise as well as the investigation of the thermodynamic continuum limit.

2.1. From microscopic to macroscopic description of cell migration with local sensing

We consider a population of motile cells within a one-dimensional domain, subject to reflecting (zero flux) boundary conditions. Each cell is considered as a discrete entity subject to logistic growth kinetics that can independently move, according to probabilistic rules, between k boxes of length $\Delta x = L/k$ on the domain $x \in [0, L]$. Hence box i constitutes the interval $[(i-1)\Delta x, i\Delta x]$ and a cell in box i sits at $x_i = (2i-1)\Delta x/2, i = 1, 2, 3, \ldots, k$. Volume exclusion is not considered as our aim is to investigate the simplest transport processes in this initial study of interfaces.

Let S_i denote the species associated with cells in box $i \in \{1, \ldots, k\}$ and define $\boldsymbol{n} = (n_1, \ldots, n_k)$ to be numbers of species $(S_1, \ldots, S_k)$ present at a given time. All changes in these species numbers can be associated with a set of transitions $T_1, \ldots, T_J$ corresponding to cell transitions between boxes and also the logistic kinetics; with a given reaction T_j, $j \in \{1, \ldots, J\}$, there is a corresponding stoichiometric vector $\boldsymbol{\nu}_j$ and propensity function $a_j(\boldsymbol{n})$, which have the following definitions:

Definition 1. The stoichiometric vector $\boldsymbol{\nu}_j = (\nu_{1j}, \ldots, \nu_{kj})$ is the state change vector of reaction T_j. Thus, if the system is in the state $\boldsymbol{n}$, and reaction T_j occurs, then the state becomes $\boldsymbol{n} + \boldsymbol{\nu}_j$ (Gillespie, 2007).

Definition 2. The propensity function $a_j(\boldsymbol{n})$ is defined to be such that $a_j(\boldsymbol{n})\, dt$ is the probability that, given the system is in state $\boldsymbol{n}$ at time t, one T_j reaction will occur within the time interval $[t, t+dt)$ for sufficiently small dt.

The propensity function has the empirical mathematical form (Gillespie, 1976)

$$a_j(\boldsymbol{n}) = k_j h_j(\boldsymbol{n}) \tag{1}$$

where (i) the function $h_j(\boldsymbol{n})$ is the number of distinct combinations of reactants contributing to the transition T_j that are available in state $\boldsymbol{n}$ and its form depends on the order of the reaction, and (ii) k_j is the specific probability rate constant and is defined to be such that $k_j dt$ is the probability that any randomly chosen reactant molecules associated with the T_j transition will undergo this transition in the next infinitesimal time interval $[t, t+dt)$.

With $P(\boldsymbol{n}, t|\boldsymbol{n}_0, t_0)$ denoting the probability that the system is in state $\boldsymbol{n}$ at time t, conditional on being in the state $\boldsymbol{n}_0$ at time t_0, a probabilistic balance yields the master equation (van Kampen, 2007; Woolley et al., 2011b)

$$\frac{\partial}{\partial t} P(\boldsymbol{n}, t|\boldsymbol{n}_0, t_0) = \sum_{j=1}^{J} P(\boldsymbol{n}-\boldsymbol{\nu}_j, t|\boldsymbol{n}_0, t_0) a_j(\boldsymbol{n}-\boldsymbol{\nu}_j) - P(\boldsymbol{n}, t|\boldsymbol{n}_0, t_0) a_j(\boldsymbol{n}). \tag{2}$$

For our specific system we consider the following $J = 4k-2$ transitions between species:

$$S_1 \underset{q_L^2}{\overset{q_R^1}{\rightleftharpoons}} S_2 \underset{q_L^3}{\overset{q_R^2}{\rightleftharpoons}} \ldots \underset{q_L^k}{\overset{q_R^{k-1}}{\rightleftharpoons}} S_k, \quad S_i \underset{p_1}{\overset{p_2}{\rightleftharpoons}} S_i + S_i, \quad i = 1 \ldots k. \tag{3}$$

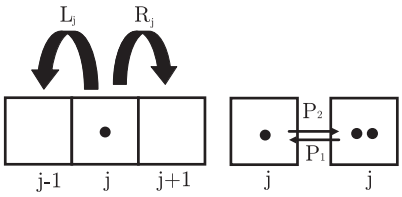

Fig. 1. Diagram of the space-jump description of diffusion and proliferation. R_j is defined as the right diffusion reaction and L_j as the left diffusion reaction. For a cell in box j, the left and right jumping stochastic coefficients are given by q_L^j and q_R^j, respectively, and the proliferation stochastic coefficient is given by p_2. For two cells in the same box, there is also the possibility of a competition induced, logistic-type, reduction in cell number with a stochastic coefficient denoted by p_1.

where $q_R^1,\ldots,q_R^{k-1},q_L^2,\ldots,q_L^k,p_1,p_2$ are stochastic transport and kinetic coefficients (see Fig. 1). Thus, the specific probability rate, denoted by k_j in Eq. (1), is given by one of the parameters $\{q_R^1,\ldots q_R^{k-1},q_L^2,\ldots,q_L^k,p_1,p_2\}$ according to the reaction under consideration. Hence the propensity functions for, respectively, right movements, left movements, proliferation and saturation induced cell loss are given by

$$q_R^1 n_1,\ldots,q_R^{k-1}n_{k-1},\quad q_L^2 n_2,\ldots,q_L^k n_k,\quad p_1 n_1,\ldots,p_1 n_k,\quad p_2 n_1^2,\ldots,p_2 n_k^2. \tag{4}$$

The stoichiometric vectors are straightforward to determine, for example the vector associated with the transitions between species $S_1\to S_2$, which simultaneously increase n_2 and decrease n_1 by one, is given by $(-1,1,0,\ldots,0)$. Hence inserting the propensity functions and stoichiometric vectors into the master equation (2), we have a stochastic representation of our system via the evolution of $P(\boldsymbol{n},t|\boldsymbol{n}_0,t_0)$ in the master equation. In particular, note from (3) that the cells are myopic, i.e. they only sense locally which, although an assumption, is a reasonable hypothesis if the length scale of the cell is much smaller than the length scale of variation of the surrounding environment. As discussed in Appendix B, this is the relevant parameter regime for a cell (without extended processes) traversing between white and grey matter, where the interfacial scale is around 100–300 μ.

2.1.1. Stochastic simulations

While the master equation provides a fundamental representation of the stochastic system, it is rarely implemented directly. For the stochastic simulations below a single realisation of the classic Gillespie algorithm (Gillespie, 1976) is implemented with unbiased motility (i.e. $q_L^i=q_R^i$ in Eq. (3) and $q_R^i=s^i$, where s^i is a signal localised to box i) via the use of Dizzy 1.11.3 (Ramsey et al., 2005), using the propensity functions and stoichiometric vectors described above. Initially, we consider 200 particles in each of the first two discrete boxes. The fact that single realisations are sufficient for our purposes below emphasises that the relatively large cell numbers associated with tumour physiology in the context of glioma are adequate to consider weak noise limits.

2.1.2. The weak noise, continuum, limit with unbiased motility

In Appendix A a detailed derivation of the continuum limit of the above stochastic system is presented in the weak noise limit using van Kampen's (2007) expansion, given unbiased motility, that is $q_R^j=q_L^j$ in Eq. (3). This derivation highlights that one must assume that the amplitude of the fluctuations scale with the inverse square root of the system size; however the saturation dynamics entails cell behaviours are not independent, preventing the use of the central limit theorem to rigorously justify this assumption. While this scaling is frequently observed even when system elements are not independent (Kubo et al., 1973) it is an explicit assumption, and thus we do need to justify the validity of the continuum approximation *a posteriori* below. Equally, the initial conditions being zero outside a compact set suggest that the expansion is not justified *a priori*.

With this caveat, and with c denoting the cell density, scaled so that the carrying capacity is unity, the result emerging from Appendix A is the continuum governing equation

$$\frac{\partial c}{\partial t}=\frac{\partial^2}{\partial x^2}\left[D\left(\frac{x}{\epsilon}\right)c\right]+c(1-c), \tag{5}$$

with zero flux boundary conditions. Note that we have non-Fickian transport. D is assumed to be a positive, smooth and bounded function for all $\epsilon>0$. For the simulations D is specified to be either of a tanh form or sinusoidal, modelling a single and multiple sharp transition regions. Further, the parameter ϵ is the ratio of the diffusive heterogeneity length scale to the reaction-diffusion length scale (i.e. $[D^*_{dim}/\rho_{dim}]^{1/2}$, where D^*_{dim} is a measure of the cellular diffusion scale and ρ_{dim} is a measure of the cellular proliferation rate). Hence, for an interface the parameter ϵ is the ratio of the interfacial length scale to $[D^*_{dim}/\rho_{dim}]^{1/2}$. Below, we consider the parameter regime $\epsilon\ll 1$ and thus focus on systems with a separation of scales, with the individual scale much smaller than that of the interface, which in turn is taken to be much smaller than the macroscopic "reaction–diffusion" length scale, $[D^*_{dim}/\rho_{dim}]^{1/2}$.

2.2. Unbiased Fickian diffusion in the continuum limit

Analogously, we can consider the microscale dynamics that is required for Fickian diffusion to emerge in the continuum limit. In particular, this does not occur for myopic sensing but necessitates that cells sense non-locally, which requires justification if the environment is changing on a much longer length scale than the cell.

For the simpler case of unbiased cell level motility, we must have stochastic transport coefficients of the form

$$q_R^i=s^i+s^{i+1},\quad q_L^i=s^i+s^{i-1},\quad i\in\{2,\ldots,k-1\}, \tag{6}$$

where s^i is a signal localised with box i and thus the above is clearly non-local. The deduction of Fickian diffusion can proceed as above and has been presented (without the complication of microscale kinetics) on numerous occasions in the literature (e.g. Baker et al., 2010).

Following such derivations with logistic kinetics and appropriate rescalings one finds

$$\frac{\partial c}{\partial t}=\frac{\partial}{\partial x}\left[D\left(\frac{x}{\epsilon}\right)\frac{\partial c}{\partial x}\right]+c(1-c), \tag{7}$$

where $D(x/\epsilon)$ is a (rescaled) continuum interpolation of $\{s_1,\ldots,s_k\}$ and ϵ inherits the above interpretation as a ratio of length scales. Finally, again note that this derivation is also subject to the same caveat that the fluctuations scale with the inverse square root of the system size, which is an explicit assumption in the presence of the non-linear kinetics that requires *a posteriori* checking.

2.3. Summary

Thus, to explore the effects of the different modelling frameworks we have four systems. Firstly for myopic cell transport we have

(i) the stochastic system associated with the master equation (2) plus the propensity functions (4) and the associated stoichiometric vectors with the assumption that left (q_L^i) and right (q_R^i) stochastic transport coefficients are equal so that the microscale dynamics is unbiased.
(ii) the continuum limit in this case, as given by Eq. (5).

For Fickian transport we instead have

(iii) the non-local stochastic system of Section 2.2 which uses propensity functions derived from Eq. (6).
(iv) Fickian diffusion in the continuum limit, Eq. (7).

Below, we always assume zero flux boundary conditions at domain edges and we explore these four systems in spatially heterogeneous environments reflecting transitions in the diffusion coefficient to observe how microscale details impact on population level behaviours in the presence of interfaces. In particular, we focus on systems with a separation of scales, with illustrations and parameter choices motivated by the context of glioma cell infiltration of white and grey matter.

3. Analytical results

We firstly analytically consider the myopic and Fickian systems in the presence of an interface to assess whether differences are generically predicted. Here, we assume D is isotropic and a function of space only. Extensions of the analytical conclusions below for more general forms of D are illustrated in Appendix C.

3.1. Fickian diffusion

We have

$$\frac{\partial c}{\partial t} = \nabla \cdot \left\{ D\left(\frac{\boldsymbol{x}}{\epsilon}\right) \nabla c \right\} + c(1-c), \tag{8}$$

where ϵ is the dimensionless length scale of the heterogeneity, i.e. it is the ratio of the diffusive heterogeneity length scale to $[D^*_{dim}/\rho_{dim}]^{1/2}$, as discussed above.

Suppose in (8) there is a single interfacial transition in the diffusion coefficient centred at a manifold C of dimensionless length scale ϵ in its normal direction, $\mathbf{n}$, which is smaller than any other length scale in the continuum model, including the radius of curvature of C. On the length scale of the transition region, the manifold C can be treated as planar and with the boundary layer rescalings $\mathbf{X} = \boldsymbol{x}/\epsilon$, $\tau = t/\epsilon^2$ we have at leading order

$$\frac{\partial c}{\partial \tau} = \frac{\partial}{\partial X}\left(D(X) \frac{\partial c}{\partial X} \right) + O(\epsilon^2), \tag{9}$$

where $X = \mathbf{X} \cdot \mathbf{n}$ and, without loss of generality, the interface is centred at $X=0$.

The variable τ is a fast time scale and yet, within the context of cellular models, the system is being driven on much slower time scales, associated with matching into the regions away from the interface, where the system is dictated by the population dynamics which does not evolve on this fast time scale. Hence, the above diffusion equation would relax to its quasi-steady state; on dropping the $O(\epsilon^2)$ correction we have

$$\frac{\partial}{\partial X}\left(D(X) \frac{\partial c}{\partial X} \right) = 0. \tag{10}$$

Integrating across the transition region twice gives

$$c(\infty) - c(-\infty) = A \int_{-\infty}^{\infty} dX \frac{1}{D(X)}$$

where A is constant. Given that the diffusion coefficient is finite and non-zero and that the population density, c, is finite, we must have $A=0$. Hence

$$c(\infty) = c(-\infty). \tag{11}$$

Thus, once any rapid transient dynamics have equilibrated, which occurs on non-dimensional time scales of $t \sim O(\epsilon^2)$ and thus much faster than the population dynamics time scale, no jump is predicted to occur across the interface. Hence, after cells initially encounter a transition region, the modelling prediction is that there is neither a sharp change in cell density across the interface nor an accumulation of cells on one side of the interface.

3.2. Myopic transport

For myopic transport, the analogue of Eq. (10) is

$$\frac{\partial^2}{\partial X^2}(D(X)c) = 0 \tag{12}$$

via an analogous derivation. Hence

$$c = \frac{AX + B}{D(X)},$$

and finiteness as $X \to \pm\infty$ enforces $A=0$ since c matches into the values of cell density either side of the interface. Thus, there is a sharp transition of cell density in the interfacial boundary layer with

$$\frac{c(-\infty)}{c(\infty)} = \frac{D(\infty)}{D(-\infty)}. \tag{13}$$

In the context of glioma, with cells moving from grey matter for $X \ll -1$ into white matter for $X \gg 1$, one has that the ratio $D(\infty)/D(-\infty)$ ranges from 5 to 25 and thus a sharp change in cell density is predicted across the interface. More generally, this emphasises that one can expect the interfacial behaviour to be very different to the Fickian case, highlighting that the microscale dynamics will have a large impact on interfacial population behaviours. This is explored in detail below via numerical simulation.

4. Numerical results

4.1. A single transition region in one spatial dimension

In Figs. 2 and 4, a single transition region in the centre of a one-dimensional spatial domain is considered for both deterministic and stochastic simulations with cells initially in a region of low diffusivity at the left of the domain. On passing through the interface the diffusivity increases by a factor of 25, as depicted in Fig. 3(a), which is consistent with an upper estimate of the ratio of cell diffusion coefficients in grey and white matter (Rockne et al., 2008; Konukoglu et al., 2010b). One can immediately note that the deterministic simulation, within the left column of the plots, accurately approximates the stochastic simulation, in the right column. Furthermore, by comparing Fig. 2 with Fig. 4, these results show a profound difference between the predictions of Fickian transport, Fig. 2, compared to myopic transport, Fig. 4. The former predicts a smooth transition through the interface with no impediment to cells; though travelling waves do not develop on this domain they are observed on larger domains (results not shown). The latter case of myopic transport, in contrast, exhibits a sharp cellular condensation in the region of the interface and a much slower penetration of cells beyond the interfacial region. Finally, we have considered different ratios of diffusion coefficients across the interface, for instance reducing the diffusion coefficient to five, and analogous results are predicted.

4.2. Multiple transition regions in one spatial dimension

In Figs. 5 and 6, transport across multiple transition regions is modelled in the case of a sinusoidal variation in the diffusion coefficient with 20 oscillations across the domain, as depicted in

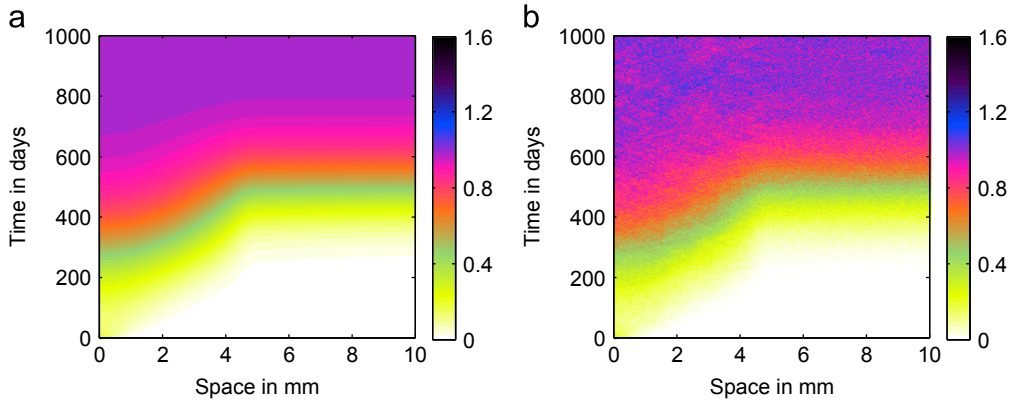

Fig. 2. Comparison of the different cases discussed in Section 2.3. Fickian transport vs stochastic simulation. Predictions from one-dimensional simulations with zero flux boundary conditions for a scaled cell density $c(x,t)$ possessing a unit carrying capacity with an initial small cell density around $x=0$, within a domain $x\in[0,10]$, where x is in units of millimetres, which is also a representative cellular reaction–diffusion length scale (see Appendix B). The dimensional diffusion coefficient, in units of mm^2 per day, is given by $D=D^+_{dim}+(D^-_{dim}-D^+_{dim})\times(1-\tanh[(x-5)/0.2])/2$, where $D^+_{dim}=0.25$ mm^2/day and $D^-_{dim}=D^+_{dim}/25$ are dimensional cellular diffusion coefficients for grey and white matter, respectively. Thus, the diffusion heterogeneity transitions sharply over an interfacial length scale of $L_{tr}\sim0.2$ mm at $x=5$ and changes by a factor of 25 with faster diffusion as x increases. Note that the square ratio of the (smallest) diffusive length scale to the length scale of the transition is given by $\epsilon^2=\rho L^2_{tr}/D_g\sim0.05$, which is within the range of parameter estimates for glioma cells given in Appendix B. (a) Result for case (iv) of Section 2.3, the Fickian continuum limit given by Eq. (7). (b) Fickian stochastic simulation, case (iii), as described in Section 2.2. We can observe that both simulations give similar results.

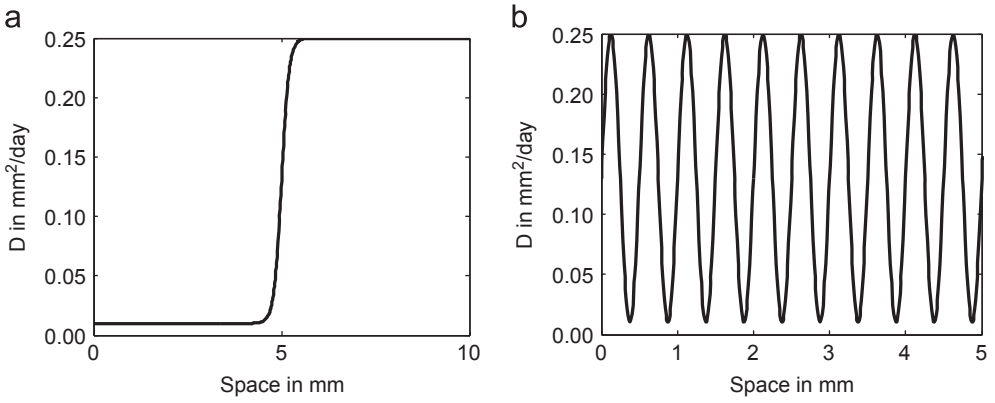

Fig. 3. Graphics of diffusion coefficients. (a) Diffusion coefficient used to obtain Figs. 2 and 4, given by $D=D^+_{dim}+(D^-_{dim}-D^+_{dim})\times(1-\tanh[(x-5)/0.2])/2$, with $D^+_{dim}=0.25$ mm^2/day and $D^-_{dim}=D^+_{dim}/25$. (b) Diffusion coefficient used to obtain Figs. 5 and 6, given by $D=(D^+_{dim}+D^-_{dim})/2+(D^+_{dim}-D^-_{dim})\sin(4\pi x)/2$, with $D^+_{dim}=0.25$ mm^2/day and $D^-_{dim}=D^+_{dim}/25$.

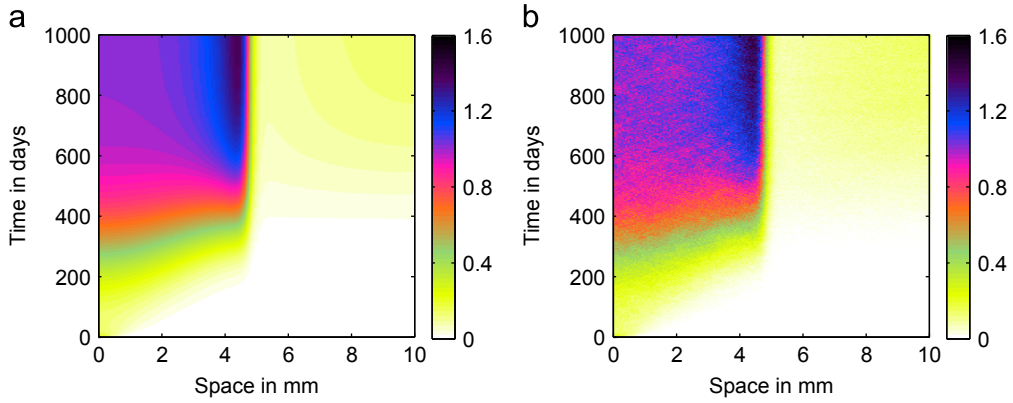

Fig. 4. Comparison of the different cases discussed in Section 2.3. Myopic transport vs stochastic simulation. Here, we have the same domain, initial conditions, boundary conditions, parameters, heterogeneous diffusion coefficient and cell kinetics as in Fig. 2. The one and only contrast is that we now have myopic cell transport. (a) Predictions of the scaled cell density $c(x,t)$ for the deterministic simulation, case (ii) given by Eq. (5). (b) The associated stochastic system, case (i), as described in Section 2.1. There exists, comparing Figs. 2 and 4, a profound difference between the predictions of Fickian transport compared to myopic transport.

Fig. 3(b), to illustrate the effects of multiple transitions regions. The left hand columns show the results from the deterministic model, while results from their stochastic analogues are presented in the right hand columns. Once more we see that noise is not important, but that there is a dramatic difference between the Fickian diffusion model, Fig. 5, and the myopic transport model,

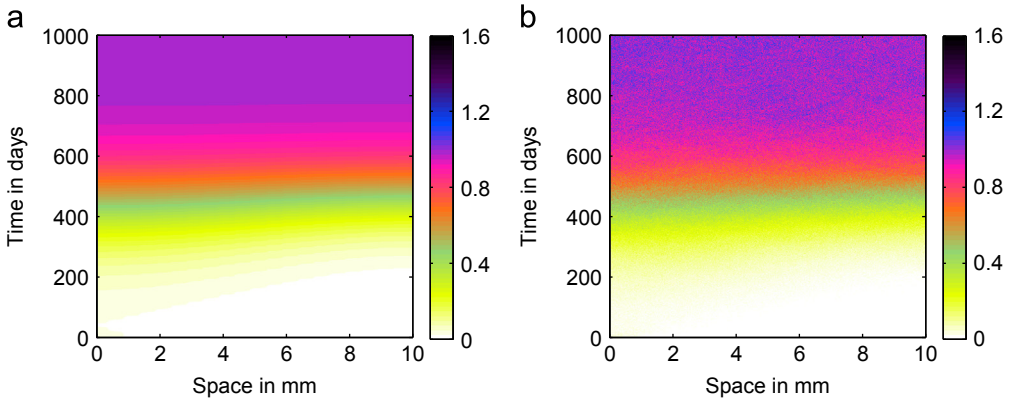

Fig. 5. Effects of oscillatory diffusion coefficient. Fickian transport. Here, we illustrate the one-dimensional simulations with zero flux boundary conditions for a scaled cell density $c(x,t)$ possessing a unit carrying capacity. There is an initial small cell density around $x=0$, within a domain $x\in[0,10]$, where x is in units of millimetres, which is also a representative cellular reaction–diffusion length scale (see Appendix B). Now, the dimensional diffusion coefficient, in units of mm^2 per day, is given by $D=(D^+_{dim}+D^-_{dim})/2+(D^+_{dim}-D^-_{dim})\sin(4\pi x)/2$, where $D^+_{dim}=0.25$ mm^2/day and $D^-_{dim}=D^+_{dim}/25$ are dimensional cellular diffusion coefficients for grey and white matter, respectively. Thus the diffusion heterogeneity transitions sharply over an interfacial length scale of L_{tr}~0.25 mm and changes by a factor of 25. Note that the square ratio of the (smallest) diffusive length scale to the length scale of the transition is given by $\epsilon^2=\rho L^2_{tr}/D^-_{dim}$~0.075, which is within the range of parameter estimates given in Appendix B. (a) The Fickian continuum limit (case (iv), Eq. (7)). (b) The associated stochastic simulation (case (iii)).

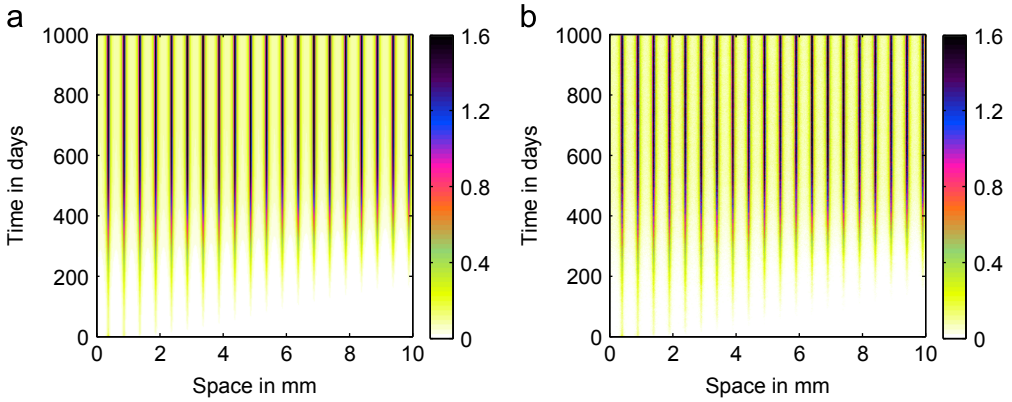

Fig. 6. Effects of oscillatory diffusion coefficient. Myopic transport. Here, we have the same domain, initial conditions, boundary conditions, parameters, heterogeneous diffusion coefficient and cell kinetics as in Fig. 5. The one and only contrast is that we now have myopic cell transport. (a) The scaled cell density $c(x,t)$ predicted by the deterministic simulation (case(ii), Eq. (5)). (b) The associated stochastic system (case (i)).

Fig. 6. Note that when extensive oscillations in the diffusion coefficient are present, as in Fig. 7, Fickian diffusion effectively homogenises the influence of the variations in the diffusion coefficient but the myopic transport model predicts a more complex dynamics with cell condensations in the transition regions. In this instance, it can also be seen that predicted infiltration speeds and time scales are similar for myopic and Fickian transport, in distinct contrast to Figs. 2 and 4.

4.3. Interfaces in two spatial dimensions

A simulation of the Fickian diffusion equation (8) with zero flux boundary conditions is presented in Fig. 8 for the scaled cell density, c, possessing a unit carrying capacity within a two-dimensional domain with a transition region in the diffusion coefficient, bisected by the black line. Here, the diffusion coefficient changes by a factor of 25, increasing in the y-direction, while the initial conditions are such that the cell density is at carrying capacity within the region enclosed by the black-dashed circle and is zero elsewhere. The explicit form of the parameters, as detailed in the caption, is motivated by glioma cell data and the scale of the white–grey matter transition (see Appendix B). Note in particular that the cell density subject to Fickian diffusion is neither hindered by the interface nor are there any sharp gradients or cell accumulations near the interface as the cells spread through the domain. Also, the relatively rapid transport of the cells in the regions associated with larger diffusion coefficient is clearly evident.

In Fig. 9 we consider myopic transport with zero flux boundary conditions in an analogous two-dimensional domain with a diffusion coefficient that again transitions sharply between the lower and upper halves of the domain. We observe predictions for a condensation of cells around the transition region, with a sharp population gradient in this region.

4.3.1. Imaging observations

Recent imaging studies (Burden-Gulley et al., 2011) not only reveal that the selected glioma cell lines extensively utilise the abluminal niche as a conduit, which we do not consider here, but also present results that appear to show that the other cell lines have sharp gradients of tumour cell accumulations that delimit grey matter–white matter interfaces, as depicted in Fig. 10. While definitive conclusions based on this initial high resolution imaging may be inappropriate as, for example, it is a single snap-shot, one can nonetheless note the analogy between the modelling and the imaging observation of Fig. 10 where the tumour cell density also

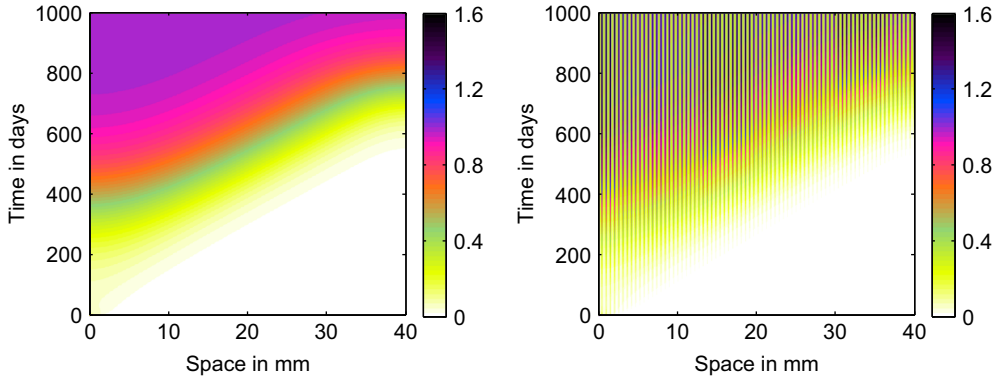

Fig. 7. Effects of oscillatory diffusion coefficient. Differences between Fickian and myopic transport. Here, we illustrate the effects of a highly oscillatory diffusion coefficient in one-dimensional simulations with zero flux boundary conditions for a scaled cell density $c(x,t)$, though now the domain is $x\in[0,40]$, where x is in units of millimetres. The dimensional diffusion coefficient, in units of mm^2 per day, is given by $D=(D^+_{dim}+D^-_{dim})/2+(D^+_{dim}-D^-_{dim})\sin(30\pi x/8)/2$, where $D^+_{dim}=0.25$ mm^2/day and $D^-_{dim}=D^+_{dim}/5$ are dimensional cellular diffusion coefficients for grey and white matter, respectively. Thus the diffusion heterogeneity transitions sharply over an interfacial length scale of L_{tr}~0.27 mm and changes by a factor of 5 with faster diffusion as x increases. Note that, as in previous figures, $\epsilon^2=\rho L^2_{tr}/D^-_{dim}$~0.03, which is within the range of parameter estimates given in Appendix B. *Left*. Fickian cell transport. *Right*: Myopic cell transport.

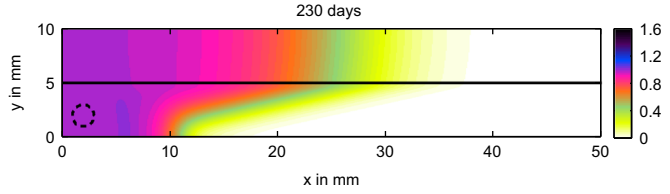

Fig. 8. A simulation of the two-dimensional Fickian diffusion equation (8) at fixed time with zero flux boundary conditions for the scaled cell density $c(x,y,t)$ possessing a unit carrying capacity. The domain is given by $x\in[0,50]$, $y\in[0,10]$, where x and y are the horizontal and vertical coordinates respectively, in units of millimetres, which is also the order of the reaction–diffusion length scale discussed in Appendix B. The dimensional diffusion coefficient, in units of mm^2 per day, is given by $D=D^+_{dim}+(D^-_{dim}-D^+_{dim})\times(1-\tanh[(y-5)/0.2])/2$, where $D^+_{dim}=0.25$ mm^2/day, $D^-_{dim}=D^+_{dim}/25$. Thus, the diffusion heterogeneity transitions sharply over an interfacial length scale of L_{tr}~0.2 mm and by a factor of 25. The square ratio of the (smallest) diffusive length scale to the length scale of the transition is given by $\epsilon^2=\rho L^2_{tr}/D^-_{dim}$~0.01, which is within the range of parameter estimates given in Appendix B. Note the region outlined by the black dashes; the initial conditions are $c=1$ inside this region, and $c=0$ elsewhere and the above plot is for $t=230$ days. Note that the density c is predicted to readily pass through the interface with no cellular accumulations. This simulation was produced using COMSOL 4.2.1.166.

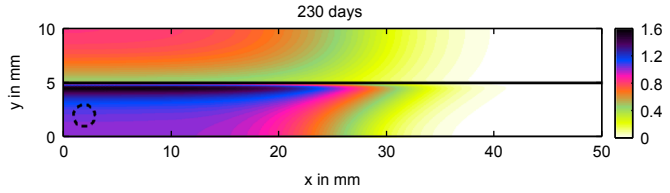

Fig. 9. A simulation of the two-dimensional generalisation for the continuum limit of the myopic equation (7) at fixed time with zero flux boundary conditions for the rescaled cell density $c(x,y,t)$ possessing a unit carrying capacity. The domain is given by $x\in[0,50]$, $y\in[0,10]$, where x and y are the horizontal and vertical coordinates, respectively, with units of millimetres, which is also a representative cellular reaction–diffusion length scale (see Appendix B). Note the region outlined by the dashed black line. The initial conditions are $c=1$ inside this region, and $c=0$ elsewhere and the above plot is for $t=230$ days. The dimensional diffusion coefficient, in units of mm^2 per day, is given by $D=D^+_{dim}+(D^-_{dim}-D^+_{dim})\times(1-\tanh[(y-5)/0.2])/2$, where $D^+_{dim}=0.25$, $D^-_{dim}=D^+_{dim}/5$ are dimensional cellular diffusion coefficients for grey and white matter, respectively. Thus the diffusion heterogeneity transitions sharply over an interfacial length scale of L_{tr}~0.2 mm and changes by a factor of 5. Note that the square ratio of the (smallest) diffusive length scale to the length scale of the transition is given by $\epsilon^2=\rho L^2_{tr}/D_g$~0.05, which is within the range of parameter estimates given in Appendix B. Clearly, the above plot demonstrates sharp transitions at the interface, and, in addition, cell condensations in this region. The simulation was produced using COMSOL 4.2.1.166.

appears to track the interface, and the very different behaviour compared with Fickian diffusion, as illustrated in Fig. 8.

5. Discussion and conclusions

In this study we have explored the behaviour of stochastic and deterministic models of cell motility, coupled with cell proliferation and logistic saturation, near interfaces. This has been motivated, in particular, by characterising how individual behaviour alters invasion through interfaces and illustrated by considering modelling frameworks for infiltrative glioma cell dynamics, where malignant tumour cells invade highly heterogeneous brain tissue.

We first observed that our simulations of the stochastic systems for relatively small cell numbers by observable tumour standards are not particularly noisy and further that van Kampen's (2007) weak noise expansion yields continuum limits with essentially the same behaviour. This is an important observation as the van Kampen expansion is based on an *ansatz* without *a priori* justification given the non-linear dynamics inherent in cell saturation. The latter introduces correlations between cells, preventing the use of rigorous results, such as the central limit theorem, to classify the scale of the system fluctuations. Thus, it cannot be guaranteed, *a priori*, to yield the correct deterministic limit. Furthermore, the infiltration speeds of the continuum limit PDEs are determined in the far field asymptotic region of the wavefront (Murray et al., 1988), precisely where the continuum approximation is strictly invalid. Despite such difficulties, one has, *a posteriori*, that continuum limits derived via van Kampen's procedure are observed to yield deterministic models that match stochastic predictions. Notably, this validates the use of continuum theory for modelling invasions in heterogeneous environments, as with simulating glioma tumour spread, despite the fact that for the continuum system, wave speed selection occurs in the asymptotic wavefront, where the continuum approximation is not strictly valid.

In these deterministic continuum limits we have analytically observed that the microscale details of cellular behaviour profoundly alter macroscale interfacial behaviours. For example, there is an absence of sharp transitions for Fickian transport, in distinct contrast to the continuum limits of myopic cellular transport, even though the analogous dynamics for both systems in homogeneous media is mathematically identical. In particular, the generality of these analytical studies emphasises that the sensitivity induced by microscale dynamics in the presence of interfaces cannot be

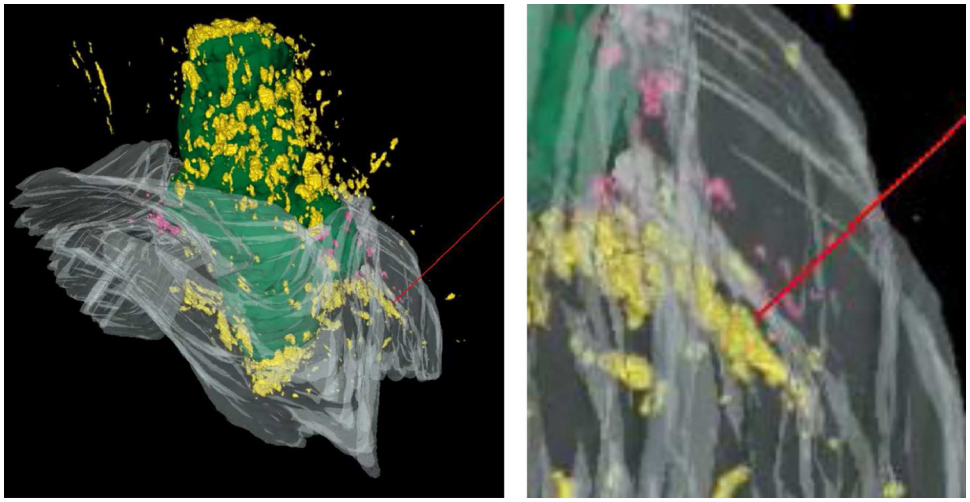

Fig. 10. Reprinted by permission from The American Association for Cancer Research: Burden-Gulley et al. (2011). Snapshot images reproduced from the supplementary material movies of Burden-Gulley et al. (2011) for high resolution imaging of the CNS-1 glioma tumour cell line within an *in vivo* mouse model. The pseudo-colour is such that green represents the core of the tumour, yellow represents dispersing cells within grey matter and pink denotes cells within the white matter, which is given by the subtle grey shading. On the left image the red line shows a mass of glioma cells delimiting the grey matter-white matter boundary, and this is magnified in the image on the right. The irregularity of the border region, and the fact that this irregularity is also present in the glioma cell density distribution, indicates that cells are accumulating at the interface rather than immediately crossing it. The fact that the interface is in a radial direction relative to the tumour core indicates that this is not simply a snap-shot of the cells before they infiltrate the white matter on spreading out from the tumour core.

resolved via different parameter choices. Similarly, the analysis presented in Appendix C illustrates that anisotropic or non-linear transport does not radically alter Fickian dynamics near an interface.

From numerical simulations, Fickian transport and its associated stochastic counterpart fail to respect interfaces, with cells predicted to readily pass through transition regions without sharp changes, exhibiting a monotonic profile with no tendency for cell accumulation. In contrast, myopic cellular transport yields a fundamentally different stochastic system and consequently a different approximate continuum limit in the presence of interfaces arising from spatial heterogeneity. Both the stochastic myopic transport system and its continuum limit exhibit sharp transitions at interfaces with cell condensations in transition regions, emphasising that cells are predicted to accumulate in these regions.

In heterogeneous media in one spatial dimension, with multiple transition regions and myopic transport, the interfaces are predicted to serve as multiple nucleation sites for the condensations of cells. Nonetheless, the invasive speed of a wavefront appears to be similar between the two modelling frameworks, as emphasised by Fig. 7. Thus, despite many quantitative differences, especially at isolated interfaces, we have also observed modelling regimes where important behaviours, such as invasion speeds, appear to be very similar between the myopic and Fickian frameworks. An intuitive explanation is that myopic transport has an additional advective term, with an advective velocity given by $\partial D/\partial x$ in one spatial dimension and $\nabla D(x/\epsilon)$ more generally, which can be readily determined by expanding the derivatives in Eq. (5). Hence, in the one-dimensional setting, wave propagation enhancements while crossing an interface from grey to white matter may be compensated when the wave passes back to grey matter from white matter, thus generating very similar invasion speeds. Nonetheless, the dynamics in higher dimensions does not indicate similarities between myopic and Fickian transport, with propagation along interfaces, illustrating that the difference in population-scale behaviour in the two models is more complex in generality. Thus further work is required to understand when individual-based behaviour produces important differences for population dynamics within heterogeneous media. Nonetheless, in the context of glioma tumour spread, these observations might suggest that the distinction between myopic and Fickian transport appears to be most relevant at white–grey matter transitions, rather than regions of the brain, such as the reticular formation, where the intermix of heterogeneity entails that a division into grey and white matter is not typically feasible (Nieuwenhuys and Donkelaar, 2003).

In higher spatial dimensions, myopic cell transport results in population level predictions of cell accumulations along interfaces between distinct homogeneous media with, in addition, cell guidance along these regions, despite the absence of anisotropic cellular transport. Further, our modelling prediction of cell guidance along interfaces is not inconsistent with the apparent predilection of CNS-1 glioma cells to accumulate at the juncture of grey and white matter in mouse (Burden-Gulley et al., 2011 and Fig. 10), in distinct contrast to Fickian-based models. These predictions also emphasise that glioma cell assays in homogeneous media provide insufficient information on cell transport to enable predictions for global behaviour *in situ* and instead more complex environments need to be considered for empirically characterising glioma cell behaviour. We close by remarking that our observations need not be restricted to glioma infiltration and more generally emphasise that individual behaviours need to be carefully assessed whenever considering population models near interfaces.

Acknowledgements

J.B.-B. would like to thank the Centre for Mathematical Biology, Mathematical Institute, Oxford for hospitality during his visit. J.B.-B. is partially supported by grants JC2010-0256 BELMONTE (Ministerio de Educación, Spain) MTM2009-13832 (Ministerio de Educación y Ciencia, Spain), MTM2012-31073 (Ministerio de Economía y Competitividad, Spain) and 0118011801 (Universidad de Castilla-La Mancha). This publication was based on work supported in part by Award No KUK-C1-013-04, made by King Abdullah University of Science and Technology (KAUST). We are grateful to an anonymous referee whose remarks were integrated into the final version of the discussion.

Appendix A. Derivation of the weak noise, continuum, limit for myopic transport

We have the master equation (2) with transitions defined by Eq. (3) and the propensity functions given by Eq. (4). Using van Kampen's (2007) expansion, we define a new random variable, $\boldsymbol{\eta}$, through the following relation:

$$\boldsymbol{n} = \boldsymbol{\phi}\Omega + \boldsymbol{\eta}\sqrt{\Omega} = \Omega\left(\boldsymbol{\phi} + \frac{1}{\sqrt{\Omega}}\boldsymbol{\eta}\right), \tag{A.1}$$

where $\boldsymbol{\eta}$ characterises the fluctuations in the species numbers and Ω is a suitable system parameter, which we take to be the initial cell number. In the absence of fluctuations, that is $\boldsymbol{\eta}=\mathbf{0}$, $\boldsymbol{\phi}=\boldsymbol{n}/\Omega$ is the weak noise limit of the number of cells per box, which can be readily scaled to give a density with unit carrying capacity. The above van Kampen *ansatz* supposes that the fluctuations scale with the square root of the number of initial cells. Given the saturation dynamics, each cell's dynamics is not independent of the other cells, and thus the central limit theorem cannot be utilised to prove the fluctuations scale in this manner. Nonetheless, it is commonly asserted that this scaling of fluctuations is apparent at statistical equilibrium, except for delicate situations such as if the system is near an unstable equilibrium point (Kubo et al., 1973). Thus we may anticipate the validity of van Kampen's *ansatz*, though this does need to be explicitly checked *a posteriori*.

Following van Kampen (2007), we can define

$$\Pi(\boldsymbol{\eta}, t) = P(\boldsymbol{n}, t)$$

using (A.1). In addition, we use the transition rates of Eq. (3) to define the macroscopic rate constants

$$d_R^i \overset{def}{=} q_R^i, \quad d_L^j \overset{def}{=} q_L^j, \quad \rho_1 \overset{def}{=} p_1, \quad \rho_2 \overset{def}{=} \Omega p_2, \tag{A.2}$$

for $i\in\{1,\ldots,k-1\}$, $j\in\{2,\ldots,k\}$ and we treat $1/\sqrt{\Omega}\ll 1$ as a small expansion parameter. d_L and d_R are the microscopic diffusion coefficients. The weak noise limit and its corrections then emerge from a regular perturbative expansion of the master equation (2), given the propensity functions of (4) and the associated stoichiometric vectors, with the additional substitution of the stochastic rate and kinetic coefficients with macroscopic rate constants of Eq. (A.2).

After extensive, but conceptually straightforward and standard algebra (Woolley et al., 2011b, 2011a), the leading order contribution to van Kampen's expansion yields the weak noise limit:

$$\frac{d\phi_1}{dt} = d_L^2\phi_2 - d_R^1\phi_1 + \rho_1\phi_1 - \rho_2\phi_1^2, \tag{A.3}$$

$$\frac{d\phi_i}{dt} = d_L^{i+1}\phi_{i+1} + d_R^{i-1}\phi_{i-1} - \left(d_R^i + d_L^i\right)\phi_i + \rho_1\phi_i - \rho_2\phi_i^2, \quad i = 2..k-1, \tag{A.4}$$

$$\frac{d\phi_k}{dt} = d_R^{k-1}\phi_{k-1} - d_L^k\phi_k + \rho_1\phi_k - \rho_2\phi_k^2. \tag{A.5}$$

In order to derive a continuum description of cell movement from the weak noise limit we expand terms such as d_L^{i+1}, d_R^{i-1} and ϕ_{i+1} about d_L^i, d_R^i and ϕ_i, respectively:

$$d_L^{i+1} = d_L(x_i+\Delta x) = d_L(x_i) + \Delta x\frac{\partial d_L}{\partial x}(x_i) + \frac{1}{2}(\Delta x)^2\frac{\partial^2 d_L}{\partial x^2}(x_i) + \cdots \tag{A.6}$$

$$d_R^{i-1} = d_R(x_i-\Delta x) = d_R(x_i) - \Delta x\frac{\partial d_R}{\partial x}(x_i) + \frac{1}{2}(\Delta x)^2\frac{\partial^2 d_R}{\partial x^2}(x_i) + \cdots \tag{A.7}$$

$$\phi_{i+1} = \phi(x_i+\Delta x) = \phi(x_i) + \Delta x\frac{\partial \phi}{\partial x}(x_i) + \frac{1}{2}(\Delta x)^2\frac{\partial^2 \phi}{\partial x^2}(x_i) + \cdots \tag{A.8}$$

where Δx is the box width. Substituting into Eqs. (A.(3), A.4) and (A.5) and taking the limit as $\Delta x\to 0$, we obtain

$$\frac{\partial\phi}{\partial t} = \frac{1}{2}\frac{\partial^2}{\partial x^2}[(D_L(x)+D_R(x))\phi] + \frac{\partial}{\partial x}[(D_L(x)-D_R(x))\phi] + \rho_1\phi - \rho_2\phi^2, \tag{A.9}$$

where

$$D_L(x)+D_R(x) = (\Delta x)^2[d_L(x)+d_R(x)], \quad D_L(x)-D_R(x) = \Delta x[d_L(x)-d_R(x)].$$

In particular, for unbiased microscale motility, as assumed below, the left and right diffusion functions are equal, $D_L(x) = D_R(x) \overset{def}{=} D(x)$, so that we have

$$\frac{\partial\phi}{\partial t} = \frac{\partial^2}{\partial x^2}[D(x)\phi] + \rho_1\phi - \rho_2\phi^2, \tag{A.10}$$

where ϕ is the cell density. A simple rescaling of the density ϕ to give a density of unit carrying capacity, denoted c, together with a rescaling of length and time, yields the continuum limit, which can be written in the form

$$\frac{\partial c}{\partial t_*} = \frac{\partial^2}{\partial x_*^2}\left[D_*\left(\frac{x_*}{\epsilon}\right)c\right] + c(1-c), \tag{A.11}$$

with zero flux boundary conditions. Here asterisks highlight rescaled variables and the parameter ϵ is the ratio of the diffusive heterogeneity length scale to the reaction–diffusion length scale (i.e. $[D^*_{dim}/\rho_{dim}]^{1/2}$, where D^*_{dim} is a measure of the cellular diffusion scale and ρ_{dim} is a measure of the cellular proliferation rate). Dropping asterisks for notational simplicity we finally have

$$\frac{\partial c}{\partial t} = \frac{\partial^2}{\partial x^2}\left[D\left(\frac{x}{\epsilon}\right)c\right] + c(1-c), \tag{A.12}$$

which represents non-Fickian transport. This transport term also arises in the Fokker–Planck approximation of lattice-free stochastic differential equation models of diffusion (Gardiner, 1985), indicating that this is not a lattice artefact of the derivation.

Appendix B. Parameter estimation

Although the mathematical formalism presented here is general we specifically consider scales pertinent to glioma invasion to fix parameters. As recognised in current modelling frameworks (Konukoglu et al., 2010a; Rockne et al., 2008; Konukoglu et al., 2010b), invading gliomas infiltrate highly heterogeneous brain tissue, due to the presence of highly disparate levels of myelin in the white and grey matter resulting in substantially different motility estimates for each phase, differing by a factor of between 5 and 25 according to the parameter estimation method (Rockne et al., 2008; Konukoglu et al., 2010b), with faster motility in white matter. Relatively few parameters are required to parameterise the model:

- D^g_{dim} and D^w_{dim}, the dimensional diffusion coefficients in grey matter and white matter, respectively.
- ρ_{dim}, the dimensional proliferation rate of cells
- L_{cell} and L_{tr}, respectively, the dimensional length scales of the cell and the interfacial transition region. Note that implicit in the analysis presented in this paper is that the scale of the cell is much smaller than that of the interface, which, in turn, is much smaller than the reaction–diffusion length scale, denoted L_D below.

A non-dimensionalisation reduces the effective number of parameters even further. We start from the dimensional deterministic Fickian equations

$$\frac{\partial c_{dim}}{\partial t_{dim}} = \frac{\partial}{\partial x_{dim}}\left(D_{dim}\left(\frac{x_{dim}}{L_{tr}}\right)\frac{\partial c_{dim}}{\partial x_{dim}}\right) + \rho_{dim}c_{dim}\left(1-\frac{c_{dim}}{K}\right),$$

Table 1
A summary of the parameter estimates.

Parameter	Interpretation	Value or Range	Comments and Citations
$D^w_{dim} \overset{def}{=} D^+_{dim}$	White matter diffusion coefficient	0.25 mm^2/day	Konukoglu et al., 2010b, Highly variable.
$D^w_{dim}/D^g_{dim} \overset{def}{=} D^+_{dim}/D^-_{dim}$	Ratio of white to grey matter diffusion coefficient	5–25	Rockne et al. (2008), Konukoglu et al. (2010b).
ρ_{dim}	Proliferation time scale	0.012/day	Konukoglu et al. (2010b), Highly variable.
L_{cell}	Cell length scale	10 μ	Glioma cell, Rouzaire-Du Bois et al. (2005).
L_{tr}	Interfacial length scale	100–300 μ	Kruggel et al. (2003), Vogt and Vogt (1919), Hellwig (1993).
ϵ^2	Squared ratio of interfacial and diffusive length scales	0.008–0.07 typically used	Wide range. Typical value based on Wang et al. (2009); Kruggel et al. (2003); Vogt and Vogt (1919); Hellwig (1993); Ellingson et al. (2011); Konukoglu et al. (2010a, 2010b); Woodward et al. (1996); Jbabdi et al. (2005).

where the diffusion coefficient varies on the length scale of the interface, L_{tr}. A simple rescaling gives the non-dimensional equations

$$\frac{\partial c}{\partial t} = \frac{1}{\epsilon^2}\frac{\partial}{\partial X}\left(D(X)\frac{\partial c}{\partial X}\right) + c(1-c) = \frac{\partial}{\partial x}\left(D\left(\frac{x}{\epsilon}\right)\frac{\partial c}{\partial x}\right) + c(1-c),$$

where $c = c_{dim}/K$, $\epsilon^2 = \rho L^2_{tr}/D^*_{dim}$, $t_{dim} = t/\rho_{dim}$, $x_{dim} = L_{tr}X$, $x = \epsilon X$ and $D = D_{dim}/D^*_{dim}$ where D^*_{dim} is a characteristic diffusion scale.

Thus, while ρ_{dim} governs the overall time scales but otherwise is unimportant in the dynamics, ϵ^2, the square ratio of the interfacial size to the reaction–diffusion length scale, $[D^*_{dim}/\rho_{dim}]^{1/2}$, is likely to be important as is the spatial dependence of the diffusion coefficient.

We proceed by estimating L_{tr} and ϵ^2, confirming that $\epsilon^2 \ll 1$, as used in the analytical investigations and numerical simulations in the main text. Firstly, high resolution magnetic resonance imaging, with voxels of length scale 0.8 mm, fails to resolve interfacial regions between white and grey matter (Rees et al., 2007); hence $L_{tr} < 0.8$ mm. In contrast, staining reveals a transition in myelin in the final layer of the grey matter cerebral cortex. The total width of the cortex is variable, but roughly 2 mm (Kruggel et al., 2003), and hence the order of the transition is around L_{tr}~100 μ, by inspection of the results of Vogt and Vogt (1919), as reported in the literature by Kruggel et al. (2003). Staining studies reported by Hellwig (1993) allow an independent estimate of this transition region to be roughly L_{tr}~300 μ.

Extensive studies have attempted to characterise the diffusive length scale associated with infiltrative gliomas

$$L_D = \sqrt{\frac{D^*_{dim}}{\rho_{dim}}}$$

where D^*_{dim} is a measure of the cellular diffusion scale and ρ_{dim} is the proliferation rate at small cell densities. In numerous theoretical studies, even the extreme estimates for L_D are nonetheless greater than 0.65 mm and are typically often 1 mm or more (e.g. Konukoglu et al., 2010a, 2010b; Woodward et al., 1996; Jbabdi et al., 2005), which, respectively, correspond to the bounds $\epsilon^2 < 0.21$ and $\epsilon^2 < 0.09$. In the patient data samples considered by Ellingson et al. (2011), one has $L_D > 1$ mm, with substantially higher values for high grade gliomas. In the sample of 32 patients considered by Wang et al. (2009), the average value of L_D was 1.1 mm, though D_{dim} ranged over three orders of magnitude in the estimates and ρ_{dim} varied by two orders of magnitude. Nonetheless, for 28 out of the 32 patients, the imaging based estimates give $L_D > 0.55$ mm, corresponding to $\epsilon^2 = 0.3$. In contrast, at the other extreme of parameter estimates, one finds a lower bound of the order of ϵ^2~0.004 (Wang et al., 2009).

Hence, for all but the extremes of the wide ranging patient data, the small ϵ regime is appropriate and also consistent with the parameter regimes of numerous previous theoretical studies. Hence we focus on parameter regimes with $\epsilon^2 \ll 1$. For definiteness, in our simulations we work with an average L_D of 1.1 mm which arises from an extensive parameter estimation study (Wang et al., 2009). Since we have upper and lower estimates of L_{tr}, i.e. 300 μ and 100 μ, we typically use

$$\left(\frac{100}{1100}\right)^2 \approx 0.008 \le \epsilon^2 \le 0.07 \approx \left(\frac{300}{1100}\right)^2.$$

In constructing the spatially heterogeneous diffusion coefficient, the details of

$$D^g_{dim} \overset{def}{=} D^-_{dim} \quad \text{and} \quad D^w_{dim} \overset{def}{=} D^+_{dim}$$

are required rather than a grouped estimate of the diffusive scale. For definiteness, we use values of D^w_{dim}~0.25 mm^2 per day, following estimates by Konukoglu et al. (2010b) with the ratio D^w_{dim}/D^g_{dim} in the range of 5–25, which is consistent with the ranges estimated in previous modelling (Rockne et al., 2008; Konukoglu et al., 2010b). Similarly, we use $\rho_{dim} = 0.012/\text{day}$ (Konukoglu et al., 2010b); though this parameter varies substantially (Wang et al., 2009), it influences only the time scales of the predictions. A summary of the parameter estimates is given in Table 1.

One further assumption that is required for model validity is that the length scale of a glial cell, L_{cell}, is much less than L_{tr}~200 μ. One observation is that L_{cell}~10 μ (Rouzaire-Du Bois et al., 2005) as required for model validity, though the models in this paper may not be readily applicable whenever migrating cells exhibit extended processes on the length scale of L_{tr} as there is no longer a separation of length scales.

Appendix C. Analysis of anisotropic nonlinear Fickian diffusion near an interface

One common generalisation of Fickian diffusion considers an anisotropy of the diffusion coefficient; a second concerns non-linear transport, whereby exclusion processes, for instance, generate nonlinearities. With $c(\boldsymbol{x}, t)$ again denoting a rescaled cell density with unit carrying capacity, these models are typically of the form

$$\frac{\partial c}{\partial t} = \frac{\partial}{\partial x_i}\left\{D_{ij}\left(\frac{\boldsymbol{x}}{\epsilon}, c\right)\frac{\partial}{\partial x_j}c\right\} + c(1-c), \tag{C.1}$$

where the summation convention is used and the diffusion coefficient is a positive, bounded and C^∞ function of the cell density (Deroulers et al., 2009; Maini et al., 2004; Sherratt and Murray, 1990; Sherratt and Marchant, 1996).

Suppose in (C.1) there is an interfacial transition in the diffusion coefficient centred at a manifold C of length scale ϵ in its normal direction, which is smaller than any other length scale in the continuum model, including the radius of curvature of C. Then, on the length scale of the transition region, the manifold C can be

treated as planar and with the boundary layer rescalings $X = x/\epsilon$, $\tau = t/\epsilon^2$ we have, at leading order, that

$$\frac{\partial c}{\partial \tau} = \frac{\partial}{\partial X}\left(\tilde{D}(X,c)\frac{\partial c}{\partial X}\right) + O(\epsilon^2) \tag{C.2}$$

within the transition region, where $\tilde{D}(X,c) = n_i D_{ij}(X,c) n_j$ is the contraction of the diffusion tensor onto the unit normal direction of the interface. The variable τ is a fast time scale and yet the system is being driven on much slower time scales, associated with matching into the regions away from the interface, where the system is dictated by the population dynamics. Hence, the above diffusion equation would relax to its quasi-steady state; on dropping the $O(\epsilon^2)$ correction we have

$$\frac{d}{dX}\left(\tilde{D}(X,c)\frac{dc}{dX}\right) = 0, \tag{C.3}$$

where, without loss of generality, the interface is centred at $X=0$.

Assuming the weak constraint that the functional form of the diffusion coefficient is separable, so that we can write it in the form $D_0(X)D_1(c)$, where both $D_0(X)$ and $D_1(c)$ are positive, smooth and bounded functions, gives us that

$$\frac{d}{dX}\left(D_0(X)\frac{dD_2(c(X))}{dX}\right) = 0, \tag{C.4}$$

where $D'_2(c) = D_1(c)$. Integrating across the transition region twice yields

$$D_2(c(\infty)) - D_2(c(-\infty)) = A\int_{-\infty}^{\infty}\frac{dX}{D_0(X)}, \tag{C.5}$$

where A is the constant of integration. The smoothness of the diffusion coefficient, and thus the requirement of boundedness for finite c, forces $A=0$, whence

$$D_2(c(\infty)) = D_2(c(-\infty)). \tag{C.6}$$

Further, from the positivity of $D_1(c)$ we have $D_2(c)$ is a monotonic increasing function of c, by its definition, and thus (C.6) is sufficient to enforce that

$$c(\infty) = c(-\infty).$$

This is valid once any rapid transient dynamics have equilibrated. Hence, after cells initially encounter a transition region, anisotropic and non-linear transport do not alter the Fickian prediction that there is neither a sharp change in cell density across the interface nor an accumulation of cells on one side of the interface (at least subject to the weak constraints that $\epsilon^2 \ll 1$ and the diffusion coefficient is separable).

References

Baker, R.E., Yates, C.A., Erban, R., 2010. From microscopic to macroscopic descriptions of cell migration on growing domains. Bull. Math. Biol. 72, 719–762.

Bearer, E.L., Lowengrub, J.S., Frieboes, H.B., Chuang, Y.L., Jin, F., Wise, S.M., Ferrari, M., Agus, D.B., Cristini, V., 2009. Multiparameter computational modeling of tumor invasion. Cancer Res. 69, 4493–4501.

Burden-Gulley, S.M., Qutaish, M.Q., Sullivant, K.E., Lu, H., Wang, J., Craig, S.E.L., Basilion, J.P., Wilson, D.L., Brady-Kalnay, S.M., 2011. Novel cryo-imaging of the glioma tumor microenvironment reveals migration and dispersal pathways in vivid three-dimensional detail. Cancer Res. 71, 5932–5940.

Chicoine, M.R., Silbergeld, D.L., 1995. Assessment of brain-tumour cell motility in-vivo and in-vitro. J. Neurosurg. 82, 615–622.

Chowdhury, D., Schadschneider, A., Nishinari, K., 2005. Physics of transport and traffic phenomena in biology: from molecular motors and cells to organisms. Phys. Life Rev. 2, 318–352.

Cronin, J.T., Reeve, W.R., Turchin, P., 2000. The pattern and range of movement of a checkered beetle predator relative to its bark beetle prey. Oikos 90, 127–138.

Deroulers, C., Aubert, M., Badoual, M., Grammaticos, B., 2009. Modeling tumor cell migration: from microscopic to macroscopic models. Phys. Rev. E 79, 031917.

Eikenberry, S.E., Sankar, T., Preul, M.C., Kostelich, E.J., Thalhauser, C.J., Kuang, Y., 2009. Virtual glioblastoma: growth, migration and treatment in a three-dimensional mathematical model. Cell Prolif. 42, 511–528.

Ellingson, B.M., LaViolette, P.S., Rand, S.D., Malkin, M.G., Connelly, J.M., Mueller, W.M., Prost, R.W., Schmainda, K.M., 2011. Spatially quantifying microscopic tumor invasion and proliferation using a voxel-wise solution to a glioma growth model and serial diffusion MRI. Magn. Reson. Med. 65, 1132–1144.

Gardiner, C.W., 1985. Handbook of Stochastic Methods. Springer, Berlin.

Gillespie, D.T., 1976. A general method for numerically simulating stochastic time evolution of coupled chemical reactions. J. Comput. Phys. 22, 403–434.

Gillespie, D.T., 2007. Stochastic simulation of chemical kinetics. Annu. Rev. Phys. Chem. 58, 35–55.

Hatzikirou, H., Deutsch, A., Schaller, C., Simon, M., Swanson, K., 2005. Mathematical modelling of glioblastoma tumour development: a review. Math. Models Method Appl. Sci. 15, 1779–1794.

Hellwig, B., 1993. How the myelin picture of the human cerebral cortex can be computed from cytoarchitectonic data. A bridge between von Economo and Vogt. J. Hirnforsch. 10, 259–269.

Hillen, T., Othmer, H.G., 2000. The diffusion limit of transport equations derived from velocity-jump processes. SIAM J. Appl. Math. 61, 751–775.

Hillen, T., Painter, K.J., 2009. A user's guide to PDE models for chemotaxis. J. Math. Biol. 58, 183–217.

Jbabdi, S., Mandonnet, E., Duffau, H., Capelle, L., Swanson, K.R., Pelegrini-Issac, M., Guillevin, R., Benali, H., 2005. Simulation of anisotropic growth of low-grade gliomas using diffusion tensor imaging. Magn. Reson. Med. 54, 616–624.

Kim, Y., Lawler, S., Nowicki, M.O., Chiocca, E.A., Friedman, A., 2009. A mathematical model for pattern formation of glioma cells outside the tumor spheroid core. J. Theor. Biol. 260, 359–371.

Konukoglu, E., Clatz, O., Bondiau, P.Y., Delingette, H., Ayache, N., 2010a. Extrapolating glioma invasion margin in brain magnetic resonance images: suggesting new irradiation margins. Med. Image Anal. 14, 111–125.

Konukoglu, E., Clatz, O., Menze, B.H., Stieltjes, B., Weber, M.A., Mandonnet, E., Delingette, H., Ayache, N., 2010b. Image guided personalization of reaction-diffusion type tumor growth models using modified anisotropic eikonal equations. IEEE Trans. Med. Imaging 29, 77–95.

Kruggel, F., Bruckner, M.K., Arendt, T., Wiggins, C.J., von Cramon, D.Y., 2003. Analyzing the neocortical fine-structure. Med. Image Anal. 7, 251–264.

Kubo, R., Matsuo, K., Kitahara, K., 1973. Fluctuation and relaxation of macrovariables. J. Stat. Phys. 9, 51–96.

Landman, K.A., Fernando, A.E., 2011. Myopic random walkers and exclusion processes: single and multispecies. Physica A 390, 3742–3753.

Lipkova, J., Zygalakis, K.C., Chapman, S.J., Erban, R., 2011. Analysis of Brownian dynamics simulations of reversible bimolecular reactions. SIAM J. Appl. Math. 71, 714–730.

Lushnikov, P.M., Chen, N., Alber, M., 2008. Macroscopic dynamics of biological cells interacting via chemotaxis and direct contact. Phys. Rev. E 78, 061904.

Maini, P.K., McElwain, D.L.S., Leavesley, D.I., 2004. Traveling wave model to interpret a wound-healing cell migration assay for human peritoneal mesothelial cells. Tissue Eng. 10, 475–482.

Moreo, P., Gaffney, E.A., Garcia-Aznar, J.M., Doblare, M., 2010. On the modelling of biological patterns with mechanochemical models: insights from analysis and computation. Bull. Math. Biol. 72, 400–431.

Murray, J.D., 2003. Mathematical Biology I: An Introduction, vol. 1, 3rd ed. Springer-Verlag.

Murray, J.D., Maini, P.K., Tranquillo, R.T., 1988. Mechanochemical models for generating biological pattern and form in development. Phys. Rep. 171, 59–84.

Nieuwenhuys, R., Donkelaar, H.J., Nicholsan C., 2003. The Central Nervous System of Vertebrates, vol. 1. Springer Verlag (Chap. 2).

Othmer, H.G., Stevens, A., 1997. Aggregation, blowup, and collapse: the ABC's of taxis in reinforced random walks. SIAM J. Appl. Math. 57, 1044–1081.

Painter, K.J., Sherratt, J.A., 2003. Modelling the movement of interacting cell populations. J. Theor. Biol. 225, 327–339.

Penington, C.J., Hughes, B.D., Landman, K.A., 2011. Building macroscale models from microscale probabilistic models: a general probabilistic approach for nonlinear diffusion and multispecies phenomena. Phys. Rev. E 84, 041120.

Ramsey, S., Orrell, D., Bolouri, H., 2005. Dizzy: stochastic simulation of large-scale genetic regulatory networks. J. Bioinf. Comput. Biol. 3, 415–436.

Rees, D., Glover, G.H., Liu, J., Wandell, B., 2007. Laminar profiles of functional activity in the human brain. Neuroimage 34, 74–84.

Rockne, R., Alvord, E.C., Szeto, M., Gu, S., Chakraborty, G., Swanson, K.R., 2008. Modeling diffusely invading brain tumors an individualized approach to quantifying glioma evolution and response to therapy. In: Selected Topics in Cancer Modeling. Modeling and Simulation in Science, Engineering and Technology, Birkhäuser, Boston, pp. 1–15.

Rouzaire-Du Bois, B., O'Regan, S., Dubois, J.M., 2005. Cell size-dependent and independent proliferation of rodent neuroblastoma x glioma cells. J. Cell Physiol. 203, 243–250.

Sherratt, J.A., Marchant, B.P., 1996. Nonsharp travelling wave fronts in the fisher equation with degenerate nonlinear diffusion. Appl. Math. Lett. 9, 33–38.

Sherratt, J.A., Murray, J.D., 1990. Models of epidermal wound healing. Proc. R. Soc. Lond. B 241, 29–36.

Stein, A.M., Demuth, T., Mobley, D., Berens, M., Sander, L.M., 2007. A mathematical model of glioblastoma tumor spheroid invasion in a three-dimensional in vitro experiment. Biophys. J. 92, 356–365.

Stupp, R., Hegi, M.E., Mason, W.P., van den Bent, M.J., Taphoorn, M.J.B., Janzer, R.C., Ludwin, S.K., Allgeier, A., Fisher, B., Belanger, K., Hau, P., Brandes, A.A., Gijtenbeek, J., Marosi, C., Vecht, C.J., Mokhtari, K., Wesseling, P., Villa, S., Eisenhauer, E., Gorlia, T., Weller, M., Lacombe, D., Cairncross, J.G., Mirimanoff, R.O., 2009. Effects of radiotherapy with concomitant and adjuvant temozolomide versus radiotherapy alone on survival in glioblastoma in a randomised

phase III study: 5-year analysis of the EORTC-NCIC trial. Lancet Oncol. 10, 459–466.
Swanson, K.R., Alvord, E.C., Murray, J.D., 2002a. Quantifying efficacy of chemotherapy of brain tumors with homogeneous and heterogeneous drug delivery. Acta Biotheor. 50, 223–237.
Swanson, K.R., Alvord, E.C., Murray, J.D., 2002b. Virtual brain tumours (gliomas) enhance the reality of medical imaging and highlight inadequacies of current therapy. Br. J. Cancer 86, 14–18.
Turchin, P., Thoeny, W.T., 1993. Quantifying dispersal of southern pine beetles with mark-recapture experiments and a diffusion model. Ecol. Appl. 3, 187–198.
van Kampen, N.G., 2007. Stochastic Processes in Physics and Chemistry, 3rd ed. North Holland.
Vogt, C., Vogt, O., 1919. Allgemeinere ergebnisse unserer hirnforschung. J. Psychiatry Neurol. 25, 279–461.
Wang, C.H., Rockhill, J.K., Mrugala, M., Peacock, D.L., Lai, A., Jusenius, K., Wardlaw, J. M., Cloughesy, T., Spence, A.M., Rockne, R., Alvord Jr., E.C., Swanson, K.R., 2009. Prognostic significance of growth kinetics in newly diagnosed glioblastomas revealed by combining serial imaging with a novel biomathematical model. Cancer Res. 69, 9133–9140.
Woodward, D.E., Cook, J., Tracqui, P., Cruywagen, G.C., Murray, J.D., Alvord, E.C., 1996. A mathematical model of glioma growth: the effect of extent of surgical resection. Cell Prolif. 29, 269–288.
Woolley, T.E., Baker, R.E., Gaffney, E.A., Maini, P.K., 2011a. Influence of stochastic domain growth on pattern nucleation for diffusive systems with internal noise. Phys. Rev. E 84, 041905.
Woolley, T.E., Baker, R.E., Gaffney, E.A., Maini, P.K., 2011b. Power spectra methods for a stochastic description of diffusion on deterministically growing domains. Phys. Rev. E 84, 021915.